Applied Physics Letters

Strain-modulated optical response in 2D $MoSe_2$ made by Na-assisted CVD on glass

Cite as: Appl. Phys. Lett. **120**, 213104 (2022); https://doi.org/10.1063/5.0090034
Submitted: 02 March 2022 • Accepted: 11 April 2022 • Published Online: 26 May 2022

João Rodrigues, Justyna Grzonka, João Fernandes, et al.

Applied Physics Letters ARTICLE scitation.org/journal/apl

Strain-modulated optical response in 2D $MoSe_2$ made by Na-assisted CVD on glass

Cite as: Appl. Phys. Lett. **120**, 213104 (2022); doi: 10.1063/5.0090034
Submitted: 2 March 2022 · Accepted: 11 April 2022 ·
Published Online: 26 May 2022

João Rodrigues,[1] Justyna Grzonka,[1] João Fernandes,[1] João Santos,[1] Oleksandr Bondarchuk,[1] Paulo Ferreira,[1,2,3] Pedro Alpuim,[1,4] and Andrea Capasso[1,a)]

AFFILIATIONS

[1]International Iberian Nanotechnology Laboratory, 4715-330 Braga, Portugal
[2]Mechanical Engineering Department and IDMEC, Instituto Superior Técnico, University of Lisbon, Av. Rovisco Pais, 1049-001 Lisboa, Portugal
[3]Materials Science and Engineering Program, University of Texas at Austin, Austin, Texas 78712, USA
[4]Centro de Física das Universidades do Minho e Porto, Universidade do Minho, 4710-057 Braga, Portugal

[a)]Author to whom correspondence should be addressed: andrea.capasso@inl.int

ABSTRACT

Extended investigations on 2D transition metal dichalcogenides (TMDCs) have opened sound possibilities to apply these materials in several technological fields such as sensing. To this end, fully reproducible methods for the wafer-scale production of crystalline and uniform 2D TMDCs are in demand. In this work, atomically thin $MoSe_2$ was grown by atmospheric-pressure chemical vapor deposition using the Na-assisted process with Se powder and Mo foil precursors on a glass substrate. The samples were extensively characterized via Raman and photoluminescence spectroscopy, atomic force microscopy, transmission electron microscopy, and x-ray photoelectron spectroscopy. The $MoSe_2$ samples consist of sub-millimeter, monolayer single-crystals with 2H phase configuration. Being monolayer and crystalline, the samples exhibit well-defined and intense photoluminescence. CVD-grown 2D $MoSe_2$ was integrated into a device with strain-tunable optical properties and tested. Under tensile strain (in the range of 0.2%–0.4%), the spectral emission responded to an in-plane strain with marked peak shifts toward lower energies for increasing levels of strain (~3 and ~2 nm shift for the main PL component at 0.2% and 0.4%, respectively), indicating a reduction of the bandgap.

Two-dimensional (2D) transition metal dichalcogenides (TMDCs) are a class of layered nanomaterials suitable for a wide range of electronic devices due to a variety of thickness-dependent electronic and optical properties.[1–6] Structurally, a TMDC layer is composed of a plane of transition metal atoms (e.g., Mo and W) in between two planes of chalcogenide atoms (e.g., S, Se, and Te) held together by strong covalent bonds. Weak interlayer van der Waals forces bind these layers along the z-direction, forming a layered crystal. Monolayer $MoSe_2$ can be applied as a photoactive layer in optoelectronics due to its intrinsic direct bandgap of ~1.5 eV, which opportunely match the visible region of the solar spectrum (400–700 nm). Several kinds of photovoltaic cells[7–10] and photodetectors[11–13] based on 2D $MoSe_2$ have been recently reported. Various techniques were proposed to change/modulate the physical properties of 2D $MoSe_2$, including doping, defect, and strain engineering, thus extending the range of application of this material. Strain engineering, in particular, allows fine-tuning of the electronic and optical properties of the 2D crystal by physically modifying its lattice and energy bands structure.[14] First-principles calculations showed that the bandgap of monolayer $MoSe_2$ should decrease by uniaxial strain (either compressive or tensile strain, 2%–10% range tested).[15] Cheng *et al.* applied progressive strain (±5%, from compression to tension) in monolayer $MoSe_2$ (produced by mechanical exfoliation) and measured the photoluminescence (PL): The optical bandgap was found to gradually decrease when the strain changed from compression to tension, and a direct-to-indirect transition occurred at a compressive strain of −1.3%. No changes were observed in the Raman spectrum under tensile strain, whereas evident changes occurred for the compressive strain.[16] PL studies on mechanically exfoliated $MoSe_2$ under uniaxial strain showed a nearly linear relationship between the strain and excitonic bandgap.[17,18] Interestingly, fluctuations in the optical bandgap energy were reported in monolayer CVD $MoSe_2$, which could be caused by the random distribution of local tensile strain, due to surface roughness and different thermal expansion coefficients between $MoSe_2$ and the substrate.[19] These effects could be potentially exploited for the fabrication of $MoSe_2$-based sensors and detectors. At present, only strain sensors (based on piezo-resistive effect) made with solution-processed $MoSe_2$

nanosheets were reported,[20,21] while no reports on the integration of CVD $MoSe_2$ in a strain sensor configuration exist.

As other TMDCs, 2D $MoSe_2$ can be grown via CVD on Si/SiO_2 substrates by evaporation of two solid precursors (i.e., Se and MoO_3 or MoO_2 powder) at suitable temperatures.[22–25] In general, CVD methods often entail reproducibility issues associated with the fine-tuning and full control of the process parameters (i.e., pressure, temperatures, and gas flow as well as precursors and substrate conditions). Other than that, the lower chemical reactivity and higher melting point of Se with respect to S make it more challenging to grow 2D $MoSe_2$ than MoS_2.[26] A CVD process to grow wafer-scale 2D $MoSe_2$ has yet to be established,[23,27,28] but recent research on salt-assisted approaches showed a pathway to reduce the melting point of the Mo-containing precursor, while increasing the reaction rate and reducing the nucleation density.[29] In particular, the use of Na as a catalyst has been recently proposed to increase the growth rate and deposited area of several TMDCs[30] (including $MoSe_2$[31]). To this end, NaCl was mixed with the metal powder and used as a precursor in the growth of submillimeter $MoSe_2$ single-crystals.[32] By a different approach, Na-containing glass was used as an "active" substrate (which released Na ions during the CVD) in the growth of MoS_2.[33–35] This approach was then applied to $MoSe_2$, leading to mm-sized, monolayer single crystals on a 6-centimeter- long soda-lime glass template (900 °C, ambient pressure).[36] Similarly, Chen *et al.* reported mm-sized, monolayer $MoSe_2$ single-crystals directly on molten soda-lime-silica glass (at 1050 °C, ambient pressure).[37] Overall, glass substrates with high amount of Na (~9.5 wt. %) appeared to promote the growth of uniform monolayer crystal.[38] Here, we have grown atomic-thin $MoSe_2$ by an innovative alkali metal-assisted approach using Se powder and Mo foil as precursors, and Na-containing glass as a substrate [Fig. 1(a)]. The approach led to monolayer $MoSe_2$ single-crystals (sizes above 100 μm) with a predominant 2H phase, showing intense PL emission. We optimized our "pick and place" method [Fig. 1(b), described in the Experimental section in the supplementary material] to transfer $MoSe_2$ crystals from glass to a flexible polydimethylsiloxane (PDMS) substrate. To this end, the PDMS substrate was exposed to water vapor to maximize the adhesion of the 2D crystal by capillary forces. When testing the CVD $MoSe_2$ crystals under uniaxial tensile strain, the PL emission was found to steadily shift toward lower energies for increasing levels of strain.[39]

2D $MoSe_2$ samples were grown via atmospheric pressure CVD (AP-CVD), as described in the Experimental section in the supplementary material. By microscopic analysis, 5–150 μm-sized polygonal single-crystals were grown [Fig. 2(a)]. They are most often isolated but coalesce into a film in some instances. This is likely due to concurrent nucleation sites, whose existence might be linked to the particle-like spots often found in the center of the crystals. Small particles surrounding the crystal edges are also visible [as indicated by the black arrows in the inset of Fig. 2(a)]. The AFM analysis shows that the $MoSe_2$ crystals are generally ~1 nm thick [Fig. 2(b)], which is a value in line with monolayer thickness (also considering that the glass surface might coarsen during CVD,

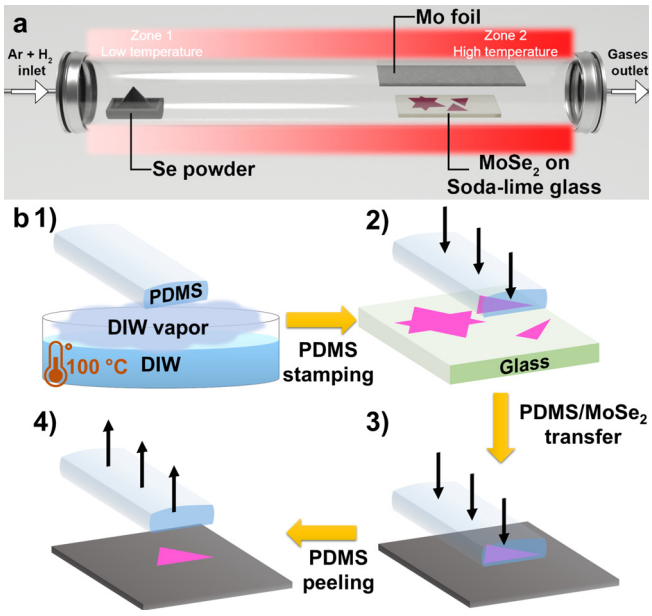

FIG. 1. (a) Schematic of the Na-assisted CVD process. (b) Sketch describing the pick and place method: (1) a viscoelastic PDMS support is exposed to water vapor for tens and lowered on top of the $MoSe_2$ crystal on glass. (2) After peeling the support from the glass substrate, the capillary forces allow one to "pick" the $MoSe_2$ crystal, which adheres to the PDMS surface. (3) By microscopic inspection, the PDMS/$MoSe_2$ stack is positioned on the desired location to "place" the crystal on the target substrate by differential adhesion. (4) The PDMS support is removed. This technique allows the dry-transfer of any 2D materials and is compatible with several types of substrates such as TEM grids.

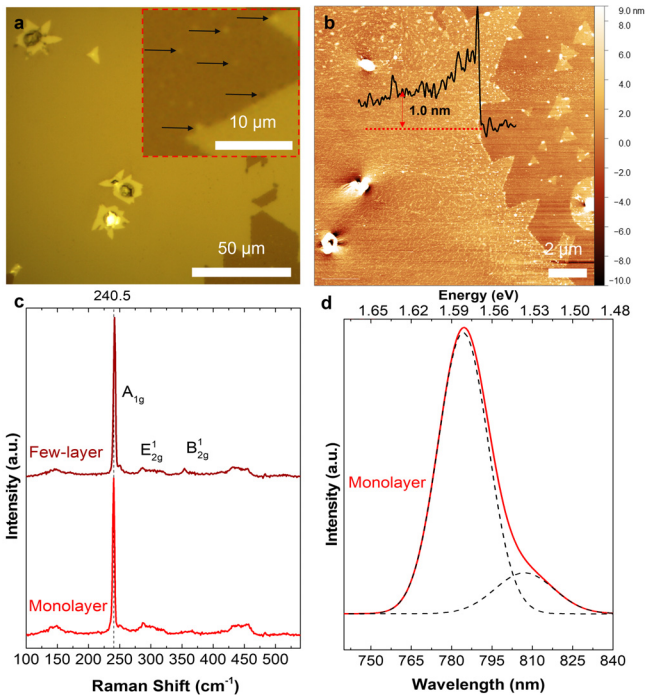

FIG. 2. (a) Optical image of the monolayer $MoSe_2$ crystals on glass, showing sporadic thicker nucleation spots. The inset shows a magnified region of the sample, highlighting small particles on the crystal edges (black arrows). (b) AFM image of the $MoSe_2$ crystal and thickness measurement. (c) Raman spectra (normalized to the A_{1g} mode intensity) of the monolayer $MoSe_2$ crystal, and a few-layer nucleation spot. (d) PL spectrum of a monolayer $MoSe_2$ crystal.

making the measurement less accurate). The samples were further evaluated by Raman spectroscopy. $MoSe_2$ usually shows two characteristic peaks related to out-of-plane (A_{1g}) and in-plane ($E_{2g}{}^1$) vibration modes. Depending on the number of layers (i.e., passing from monolayer to bulk), these modes vary in position: from 240.5 to 242.5 cm^{-1} and from 287.2 to 286 cm^{-1}, respectively.[40] Figure 2(c) shows the vibrational modes in the range of interest. A main A_{1g} mode at 240.5 cm^{-1} stands out, which is indicative of monolayer thickness for the single-crystals. In the sporadic regions with secondary nucleation (often hosting a small particle), the A_{1g} mode blue-shifts to 241.7 cm^{-1}, pointing at a few-layer thickness. A very small peak at ~250 cm^{-1} [Fig. 2(c)] can be seen, which could be related to minor disorder such as Se vacancies or other crystallographic defects.[41] A close-up analysis of the A_{1g}, $E_{2g}{}^1$ and $B_{2g}{}^1$ modes is given in Fig. S1. The PL spectrum of the $MoSe_2$ crystal [Fig. 2(d)] could be fitted with two components: a first one related to the neutral exciton A^0 and a second one at a lower energy (generally related to a trion).[19] This is different from mechanically exfoliated $MoSe_2$, which usually shows a single, symmetric PL peak.[17,18] The main component appears at ~784 nm and is slightly red-shifted with respect to mechanically exfoliated samples (790 nm).[40] The second component is located at ~807 nm. In terms of optical absorbance, the two expected excitonic peaks appear (A and B, Fig. S2). Their positions (~785 and 690 nm) are also redshifted with respect to the literature (~794 and 700 nm).[42] The red-shifts observed in PL and optical absorbance peaks could be connected to a minor strain in the $MoSe_2$ crystals, induced by the heating/cooling process of the glass substrate.[16] The $MoSe_2$ crystals on glass were analyzed by x-ray photoelectron spectroscopy (XPS) to ascertain the elemental composition [Fig. S3(a)]. Figure S3(b) shows the high-resolution spectrum of Mo3d, which consists of two main peaks with binding energies of ~228.5 and ~231.7 eV (corresponding to $Mo3d_{5/2}$ and $Mo3d_{3/2}$, respectively). Figure S3(c) shows the high-resolution spectrum of Se3d with two peaks at ~54.1 and ~55 eV corresponding to divalent Se ions ($Se\ 3d_{5/2}$ and $3d_{3/2}$, respectively). Interestingly, the position and width of the main peaks in the Mo3d and Se3d spectra confirm the presence of the sole 2H phase (no 1T phase). These characteristics are in line with the literature on CVD $MoSe_2$.[12,22,43,44]

A detailed TEM analysis was employed to ascertain the atomic structures of the $MoSe_2$ crystals. Figure 3(a) shows triangular-shaped $MoSe_2$ crystals transferred on TEM grids. Figure 3(b) shows a high-angle annular dark-field imaging (HAADF) scanning transmission electron microscopy (STEM) image of their inner structure. The fast Fourier transformation (FFT) shown in the inset confirms the single-crystal form of $MoSe_2$. A few defects can be found in the crystals, as shown within the white square in Fig. 3(c). These triangular voids can appear in either

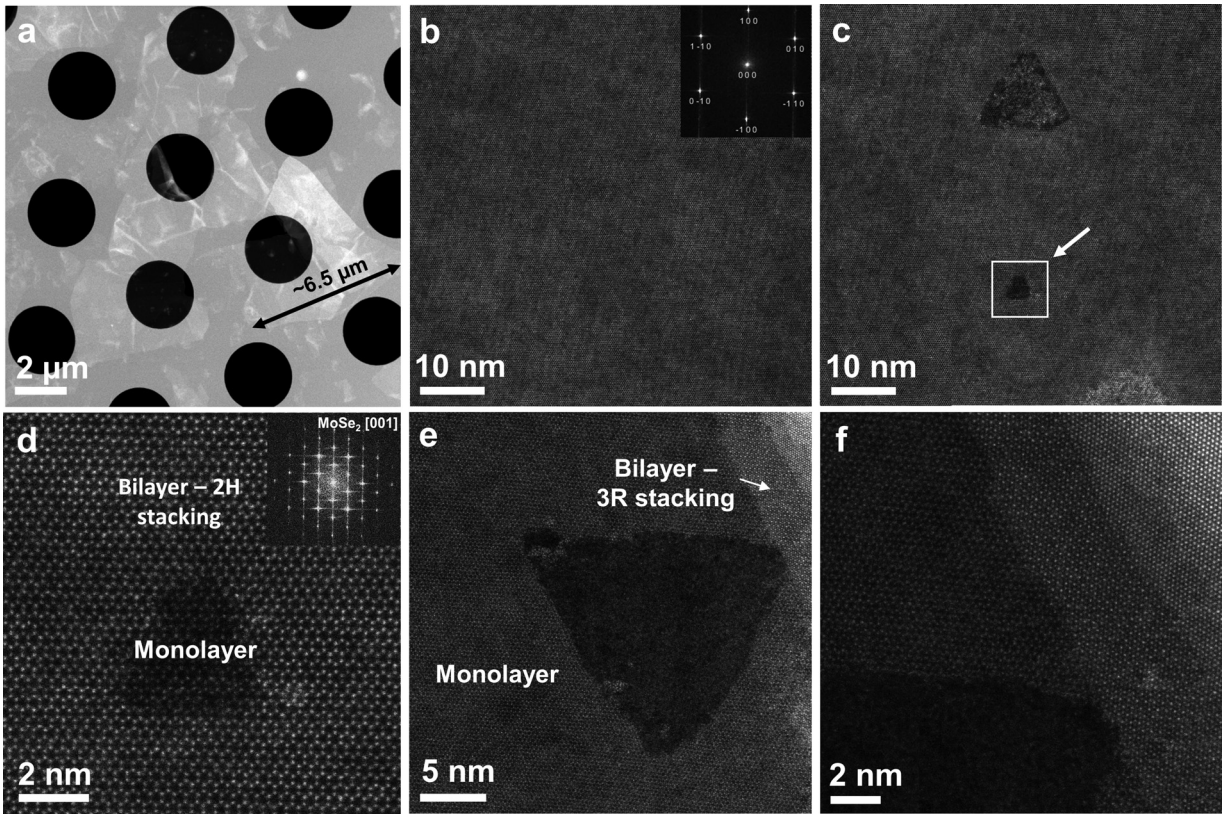

FIG. 3. (a) HAADF STEM image highlighting a triangular $MoSe_2$ crystal with lateral size of ~6.5 μm. (b) HAADF STEM image of the crystal in (a) and corresponding FFT (inset), confirming the crystalline structure of $MoSe_2$. (c) HAADF STEM image showing two defects in the single crystal (dark triangular regions). The region within the white square is depicted in detail in (d) which shows a HAADF STEM image of a triangle-shaped defect (monolayer) in bilayer $MoSe_2$ with 2H stacking. (e) HAADF STEM image of a triangle-shaped defect in monolayer $MoSe_2$, next to a bilayer with 3R stacking. (f) Higher magnification image of (e), showing a hole in monolayer $MoSe_2$.

monolayer [Figs. 3(d) and 3(e)] or bilayer [with 2H stacking, Fig. 3(f)] regions of the crystal.[27] In the CVD of 2D TMDCs, molten salts as NaCl are known to increase the reaction rate by reducing the melting point of the metal precursors and increasing the mass flux of vaporized precursors.[30] By our CVD approach (i.e., using a Mo foil and a glass substrate), small amounts of Na are released from the glass and interact with the Mo foil, inducing corrosion: This, in turn, would increase the reactivity and volatilization of Mo atoms.[45–47] The Mo foil precursor, in lieu of the Mo oxide powder, thus, assures a uniform Mo supply, fostering a large-scale growth as previously observed for MoS_2.[35,48] Overall, in contrast with common two-powder precursor approaches, our growth method offers a much higher control on the 2D crystal formation, which ends up in atomic-thick, polygonal (e.g., triangular and hexagonal) crystals.

Following the transfer of monolayer $MoSe_2$ crystals to a flexible PDMS substrate, we investigated their optoelectronic properties under uniaxial tensile strain using a custom-made setup [Fig. 4(a)]. Figure 4(b) shows the $MoSe_2$ crystal under test. Raman and PL measurements were acquired in a strain range 0%–0.4% (estimated as reported in Ref. 49). The Raman spectra remain unaltered regardless of the applied strain: In all cases, the A_{1g} peak vibration is centered at 240.5 cm^{-1}, as expected for monolayer $MoSe_2$ [Fig. 4(c)].[16] The situation is different for the PL, as shown in Fig. 4(d). The PL spectra of $MoSe_2$ on PDMS are broader than those acquired on glass, mostly due to a significant FWHF increase in the second component (~57 vs ~21 nm). This could be due to defects induced in the crystal by the dry-transfer process.[50] After transfer to PDMS, the first component remains in the same position (~784 nm), while the second red-shifts to ~807 nm (vs 797 nm). The second component appears sensitive to the mechanical deformation: This could be explained by a stress relaxation occurring after transferring the crystals from the native glass to PDMS. At a 0.2% strain, a red-shift in both components is observed with the second one experiencing again the larger shift (+3, +16 nm, respectively). At a 0.4% strain, a blue-shift in the components take place (−1, −7 nm, respectively). Finally, when recovering to a flat state, a further slight blue-shift occurs (−2, −2 nm): Overall, the first component goes back to the initial value, while the second stays red-shifted by 7 nm.

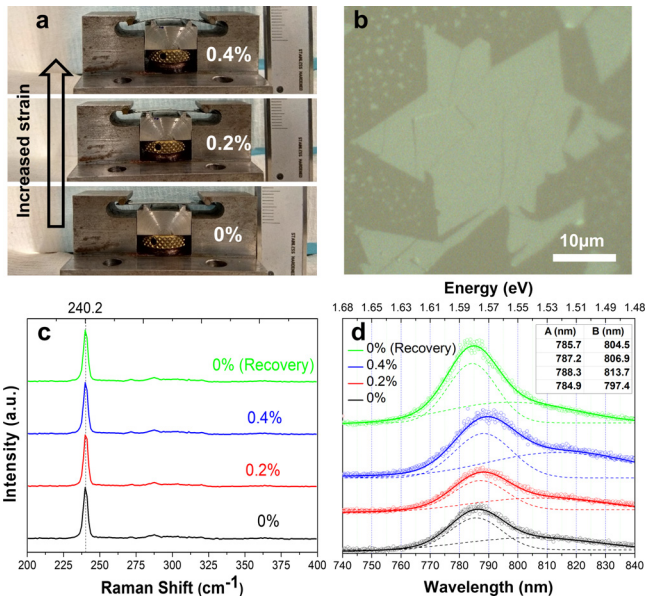

FIG. 4. (a) Photograph of the custom-made setup used to apply external strain to the $MoSe_2$ crystals. (b) Optical microscope image of the as-transferred $MoSe_2$ crystal on PDMS. (c) Raman and (d) PL plots of the $MoSe_2$ crystal acquired at different strain levels.

The observed shifts in PL peak positions can be attributed to tension-induced change in the lattice parameter, which modifies the electronic band structure and bandgap energy. In mechanically exfoliated, monolayer $MoSe_2$, a 1% of strain was reported to reduce the bandgap energy by ~30–40 meV.[17,18] Assuming a linear behavior, a 0.2% strain would translate in a reduction of 6–8 meV, which match the 6.7 meV reduction we measured in the main PL component (equivalent to the 3 nm shift).[16,18] In summary, our innovative Na-assisted route (using Se powder and Mo foil precursors) led to the growth of monolayer $MoSe_2$ single-crystals with sizes above 100 μm on glass. We transfer the crystals to desired locations on flexible PDMS by a pick and place method without compromising their structural integrity and optoelectronic properties. In this way, we could test the photoluminescence of the crystals under uniaxial tensile strain, highlighting the peak shift at different strain levels. These results lay the ground in view of 2D $MoSe_2$-based strain sensing devices.

See the supplementary material for experimental procedures, detailed Raman analysis, optical absorbance, and XPS of the 2D $MoSe_2$.

We acknowledge the financial support of the project "GEMIS—Graphene-enhanced Electro Magnetic Interference Shielding" with Reference No. POCI-01-0247-FEDER-045939, co-funded by COMPETE 2020—Operational Programme for Competitiveness and Internationalization and FCT—Science and Technology Foundation, under the Portugal 2020 Partnership Agreement, through the European Regional Development Fund. This work was supported by FCT, through IDMEC-Mechanical Engineering Institute, under LAETA-Associate Laboratory of Energy, Transports and Aeronautics, Project No. UIDB/50022/2020 and via the Strategic Funding UIDB/04650/2020. We thank Dr. S. Sadewasser and Mr. B. Baumgartner for their assistance in preliminary experiments.

AUTHOR DECLARATIONS

Conflict of Interest

The authors have no conflicts to disclose.

DATA AVAILABILITY

The data that support the findings of this study are available from the corresponding author upon reasonable request.

REFERENCES

[1]B. Radisavljevic, A. Radenovic, J. Brivio, V. Giacometti, and A. Kis, Nat. Nanotechnol. **6**, 147 (2011).
[2]O. Lopez-Sanchez, D. Lembke, M. Kayci, A. Radenovic, and A. Kis, Nat. Nanotechnol. **8**, 497 (2013).
[3]R. Cheng, D. Li, H. Zhou, C. Wang, A. Yin, S. Jiang, Y. Liu, Y. Chen, Y. Huang, and X. Duan, Nano Lett. **14**, 5590 (2014).
[4]M. L. Tsai, S. H. Su, J. K. Chang, D. S. Tsai, C. H. Chen, C. I. Wu, L. J. Li, L. J. Chen, and J. H. He, ACS Nano **8**, 8317 (2014).

[5]M. Dubey, L.-J. Li, M. L. Chin, J. Kong, T. Palacios, L. Yu, Y.-H. Lee, A. Hsu, Y. Shi, and H. Wang, Nano Lett. **12**, 4674 (2012).
[6]S. Kang, D. Lee, J. Kim, A. Capasso, H. S. Kang, J. W. Park, C. H. Lee, and G. H. Lee, 2D Mater. **7**, 022003 (2020).
[7]P. De Sarkar, A. Paul, and K. K. Ghosh, IOSR J. Electron. Commun. Eng. **12**, 13 (2017).
[8]K. J. Hsiao, J. Da Liu, H. H. Hsieh, and T. S. Jiang, Phys. Chem. Chem. Phys. **15**, 18174 (2013).
[9]A. Capasso, F. Matteocci, L. Najafi, M. Prato, J. Buha, L. Cinà, V. Pellegrini, A. D. Carlo, and F. Bonaccorso, Adv. Energy Mater. **6**, 1600920 (2016).
[10]S. Bellani, L. Najafi, A. Capasso, A. E. Del Rio Castillo, M. R. Antognazza, and F. Bonaccorso, J. Mater. Chem. A **5**, 4384–4396 (2017).
[11]W. Du, P. Yu, J. Zhu, C. Li, H. Xu, J. Zou, C. Wu, Q. Wen, H. Ji, T. Liu, Y. Li, G. Zou, J. Wu, and Z. M. Wang, Nanotechnology **31**, 225201 (2020).
[12]Y. H. Chang, W. Zhang, Y. Zhu, Y. Han, J. Pu, J. K. Chang, W. T. Hsu, J. K. Huang, C. L. Hsu, M. H. Chiu, T. Takenobu, H. Li, C. I. Wu, W. H. Chang, A. Wee, and L. J. Li, ACS Nano **8**, 8582 (2014).
[13]V. Selamneni, N. Nerurkar, and P. Sahatiya, IEEE Sens. Lett. **4**, 1–4 (2020).
[14]D. Akinwande, N. Petrone, and J. Hone, Nat. Commun. **5**, 5678 (2014).
[15]Y. Tian, A. Sun, Z. Ge, Y. Zhang, S. Huang, S. Lv, and H. Li, Chem. Phys. Lett. **765**, 138286 (2021).
[16]X. Cheng, L. Jiang, Y. Li, H. Zhang, C. Hu, S. Xie, M. Liu, and Z. Qi, Appl. Surf. Sci. **521**, 146398 (2020).
[17]J. Ji, A. Zhang, T. Xia, P. Gao, Y. Jie, Q. Zhang, and Q. Zhang, Chin. Phys. B **25**, 013602 (2016).
[18]J. O. Island, A. Kuc, E. H. Diependaal, R. Bratschitsch, H. S. Van Der Zant, T. Heine, and A. Castellanos-Gomez, Nanoscale **8**, 2589 (2016).
[19]J. Krustok, T. Raadik, R. Jaaniso, V. Kiisk, I. Sildos, M. Marandi, H. P. Komsa, B. Li, X. Zhang, Y. Gong, and P. M. Ajayan, Appl. Phys. Lett. **109**, 253106 (2016).
[20]P. M. Pataniya, S. A. Bhakhar, M. Tannarana, C. Zankat, V. Patel, G. K. Solanki, K. D. Patel, P. K. Jha, D. J. Late, and C. K. Sumesh, J. Colloid Interface Sci. **584**, 495 (2021).
[21]V. Selamneni, S. K. Ganeshan, N. Nerurkar, T. Akshaya, and P. Sahatiya, IEEE Trans. Instrum. Meas. **70**, 1–8 (2021).
[22]Y. Zhao, H. Lee, W. Choi, W. Fei, and C. J. Lee, RSC Adv. **7**, 27969 (2017).
[23]X. Lu, M. I. B. Utama, J. Lin, X. Gong, J. Zhang, Y. Zhao, S. T. Pantelides, J. Wang, Z. Dong, Z. Liu, W. Zhou, and Q. Xiong, Nano Lett. **14**, 2419 (2014).
[24]S. Wang, G. Wang, X. Yang, H. Yang, M. Zhu, S. Zhang, G. Peng, and Z. Li, Nanomaterials **10**, 75 (2020).
[25]Y. Jung, E. Ji, A. Capasso, and G.-H. Lee, J. Korean Ceram. Soc. **56**, 24–36 (2019).
[26]A. Eftekhari, Appl. Mater. Today **8**, 1–17 (2017).
[27]Y. Gong, G. Ye, S. Lei, G. Shi, Y. He, J. Lin, X. Zhang, R. Vajtai, S. T. Pantelides, W. Zhou, B. Li, and P. M. Ajayan, Adv. Funct. Mater. **26**, 2009 (2016).
[28]H. Wang, D. Zhu, F. Jiang, P. Zhao, H. Wang, Z. Zhang, X. Chen, and C. Jin, Nanotechnology **29**, 314001 (2018).
[29]C. Xie, P. Yang, Y. Huan, F. Cui, and Y. Zhang, Dalton Trans. **49**, 10319 (2020).
[30]J. Zhou, J. Lin, X. Huang, Y. Zhou, Y. Chen, J. Xia, H. Wang, Y. Xie, H. Yu, J. Lei, D. Wu, F. Liu, Q. Fu, Q. Zeng, C. H. Hsu, C. Yang, L. Lu, T. Yu, Z. Shen, H. Lin, B. I. Yakobson, Q. Liu, K. Suenaga, G. Liu, and Z. Liu, Nature **556**, 355–359 (2018).
[31]T. Chen, G. Hao, G. Wang, B. Li, L. Kou, H. Yang, X. Zheng, and J. Zhong, 2D Mater. **6**, 025002 (2019).
[32]J. Li, W. Yan, Y. Lv, J. Leng, D. Zhang, C. O. Coileaín, C. P. Cullen, T. Stimpel-Lindner, G. S. Duesberg, J. Cho, M. Choi, B. S. Chun, Y. Zhao, C. Lv, S. K. Arora, and H. C. Wu, RSC Adv. **10**, 1580 (2020).
[33]H. Kim, D. Ovchinnikov, D. Deiana, D. Unuchek, and A. Kis, Nano Lett. **17**, 5056 (2017).
[34]P. Yang, Z. Zhang, M. Sun, F. Lin, T. Cheng, J. Shi, C. Xie, Y. Shi, S. Jiang, Y. Huan, P. Liu, F. Ding, C. Xiong, D. Xie, and Y. Zhang, ACS Nano **13**, 3649 (2019).
[35]P. Yang, X. Zou, Z. Zhang, M. Hong, J. Shi, S. Chen, J. Shu, L. Zhao, S. Jiang, X. Zhou, Y. Huan, C. Xie, P. Gao, Q. Chen, Q. Zhang, Z. Liu, and Y. Zhang, Nat. Commun. **9**, 979 (2018).
[36]Z. Zhang, L. Zhu, D. Wang, B. Tang, P. Yang, Y. Shi, F. Zhou, J. Fu, Y. Huan, F. Cui, N. Li, Q. Chen, X. Zou, F. Chen, and Y. Zhang, Adv. Mater. Interfaces **8**, 2170069 (2021).
[37]J. Chen, X. Zhao, S. Tan, H. Xu, B. Wu, B. Liu, D. Fu, W. Fu, D. Geng, Y. Liu, W. Liu, W. Tang, L. Li, W. Zhou, T. C. Sum, and K. P. Loh, J. Am. Chem. Soc. **139**, 1073 (2017).
[38]G. U. Özküçük, C. Odacı, E. Şahin, F. Ay, and N. K. Perkgöz, Mater. Sci. Semicond. Process. **105**, 104679 (2020).
[39]B. Silva, J. Rodrigues, B. Sompalle, C.-D. Liao, N. Nicoara, J. Borme, F. Cerqueira, M. Claro, S. Sadewasser, P. Alpuim, and A. Capasso, Nanomaterials **11**, 1650 (2021).
[40]P. Tonndorf, R. Schmidt, P. Bottger, X. Zhang, J. Borner, A. Liebig, M. Albrecht, C. Kloc, O. Gordan, D. R. T. Zahn, S. M. De Vasconcellos, and R. Bratschitsch, in 2013 Conference on Lasers and Electro Optics, 2013.
[41]Zhao, X. X., Ji, Y. J., Chen, J. Y., Fu, W., Dan, J. D., Liu, Y., Pennycook, S. J., Zhou, W., and Loh, K. P., Adv. Mater. **31**, 1900237 (2019).
[42]S.-H. Su, W.-T. Hsu, C.-L. Hsu, C.-H. Chen, M.-H. Chiu, Y.-C. Lin, W.-H. Chang, K. Suenaga, J.-H. He, and L.-J. Li, Front. Energy Res. **2**, 27 (2014).
[43]E. D. Hanson, L. M. Lilley, J. D. Cain, S. Hao, E. Palacios, K. Aydin, C. Wolverton, T. Meade, and V. P. Dravid, Mater. Chem. Phys. **225**, 219 (2019).
[44]X. Wang, Y. Gong, G. Shi, W. L. Chow, K. Keyshar, G. Ye, R. Vajtai, J. Lou, Z. Liu, E. Ringe, B. K. Tay, and P. M. Ajayan, ACS Nano **8**, 5125–5131 (2014).
[45]J. Chen, X. Zhao, G. Grinblat, Z. Chen, S. Tan, W. Fu, Z. Ding, I. Abdelwahab, Y. Li, D. Geng, Y. Liu, K. Leng, B. Liu, W. Liu, W. Tang, S. A. Maier, S. J. Pennycook, and K. P. Loh, Adv. Mater. **30**, 1704674 (2018).
[46]V. V. Karpov, A. V. Abramov, A. Y. Zhilyakov, S. V. Belikov, V. A. Volkovich, I. B. Polovov, and O. I. Rebrin, AIP Conf. Proc. **1767**, 020011 (2016).
[47]J. Liu, L. Lei, C. Peng, M. Jiang, Y. Wang, and Z. Wu, Phys. Chem. Glasses: Eur. J. Glass Sci. Technol., Part B **56**, 212 (2015).
[48]J. Zheng, X. Yan, Z. Lu, H. Qiu, G. Xu, X. Zhou, P. Wang, X. Pan, K. Liu, and L. Jiao, Adv. Mater. **29**, 1604540 (2017).
[49]R. Roldán, A. Castellanos-Gomez, E. Cappelluti, and F. Guinea, J. Phys.: Condens. Matter **27**, 313201 (2015).
[50]P. K. Chow, R. B. Jacobs-Gedrim, J. Gao, T. M. Lu, B. Yu, H. Terrones, and N. Koratkar, ACS Nano **9**, 1520 (2015).